Classic OFDM Systems and Pulse Shaping OFDM/OQAM Systems

Jinfeng Du, Svante Signell

February 2007

Electronic, Computer, and Software Systems
Information and Communication Technology
KTH - Royal Institute of Technology
SE-100 44 Stockholm, Sweden

TRITA-ICT/ECS R 07:01
ISSN 1653-7238
ISRN KTH/ICT/ECS/R-07/01–SE

Classic OFDM Systems and Pulse Shaping OFDM/OQAM Systems

Jinfeng Du, Svante Signell

February 2007

Electronic, Computer, and Software Systems
Information and Communication Technology
KTH - Royal Institute of Technology
SE-100 44 Stockholm, Sweden

TRITA-ICT/ECS R 07:01
ISSN 1653-7238
ISRN KTH/ICT/ECS/R-07/01–SE

Abstract

In this report, we provide a comparative study of state-of-the-art in Orthogonal Frequency Division Multiplexing (OFDM) techniques with orthonormal analysis and synthesis basis. Two main categories, OFDM/QAM which adopts baseband Quadrature Amplitude Modulation (QAM) and rectangular pulse shape, and OFDM/OQAM which uses baseband offset QAM and various pulse shapes, are intensively reviewed. OFDM/QAM can provide high data rate communication and effectively remove intersymbol interference (ISI) by employing guard interval, which costs a loss of spectral efficiency and increases power consumption. Meanwhile it remains very sensitive to frequency offset which causes intercarrier interference (ICI). In order to achieve better spectral efficiency and reducing combined ISI/ICI, OFDM/OQAM using well designed pulses with proper Time Frequency Localization (TFL) is of great interest. Various prototype functions, such as rectangular, half cosine, Isotropic Orthogonal Transfer Algorithm (IOTA) function and Extended Gaussian Functions (EGF) are discussed and simulation results are provided to illustrate the TFL properties by the ambiguity function and the interference function.

Contents

1 Introduction

OFDM, orthogonal frequency division multiplexing, is an efficient technology for wireless communications. It is widely used in many of the current and coming wireless and wireline standards, e.g., VDSL, DAB, DVB-T, WLAN (IEEE 802.11a/g), WiMAX (IEEE 802.16), 3G LTE and others as well as the 4G wireless standard, since next generation wireless systems will be fully or partially OFDM-based.

The classic OFDM employing baseband quadrature amplitude modulation and rectangular pulse shape, denoted OFDM/QAM, is most commonly used in today's applications which refers to OFDM. In an ideal channel where no frequency offset is induced, intercarrier interference (ICI) can be fully removed by orthogonality between sub-carriers. Intersymbol interference (ISI), which is caused by multipath propagation, can also be eliminated by adding a guard interval (i.e., a cyclic prefix after OFDM modulation[1]) which is longer than the maximum time dispersion. On the other hand, such guard interval (cyclic prefix) costs a loss of spectral efficiency and increases power consumption.

In order to achieve better spectral efficiency and meanwhile reducing combined ISI/ICI, another OFDM scheme using *offset* QAM for each sub-carrier, denoted OFDM/OQAM, is of increasing importance as it has already illustrated profound advantage [1, 2, 3] over OFDM/QAM in time and frequency dispersive channels. Contrary to OFDM/QAM which modulates each sub-carrier with a complex-valued symbol, OFDM/OQAM modulation carriers a real-valued symbol in each sub-carrier and consequently allows time-frequency well localized pulse shape under denser system TFL requirement. The well designed IOTA pulse has already been introduced in the TIA's Digital Radio Technical Standards [6] and been considered in WRAN(IEEE 802.22) [7].

By adopting various pulse shaping prototype functions [1]-[5] with *good*[2] time frequency localization (TFL) property, OFDM/OQAM can efficiently reduce both ISI and ICI without employing any guard interval. This enables a very efficient packing of time-frequency symbols maximizing e.g. the throughput or the interference robustness in the communication link.

Our aim in this report, motivated by [8], is to provide a comparative study of state-of-the-art in OFDM techniques with orthonormal analysis and synthesis basis which consists of the time-frequency translated versions of the prototype function. Section 2 gives an overview of principles and architecture of the classical OFDM/QAM scheme and provide a basis for further discussion. OFDM/OQAM scheme with pulse shaping as well as several prototype functions like rectangular, half-cosine, Gaussian, IOTA and EGF are present in Section 3. In Section 4, the ambiguity function and interference function for TFL analysis are applied to provide different prototype functions. Some simulation results are presented in Section 5 and conclusions and extensions for OFDM are presented in Section 6.

[1] see Sec. 2 for detailed explanation.

[2] The criteria of *good* will be discussed later in Sec. 3

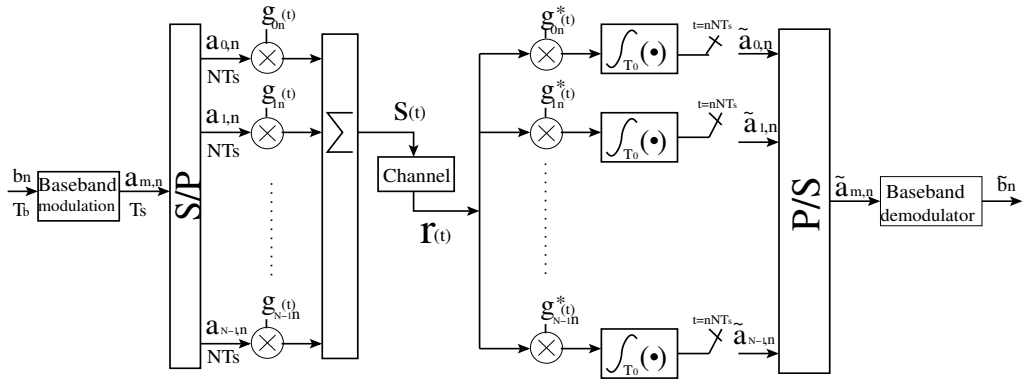

Figure 1: Block diagram of OFDM/QAM system (equivalent lowpass).

2 OFDM/QAM and Cyclic Prefix

The main idea behind OFDM is to partition the frequency selective fading channel (time dispersion T_d is larger than symbol duration T_s) into a large number (say N) of parallel sub-channels which are flat fading ($T_d << NT_s$) and thereafter transform a very high data rate ($\frac{1}{T_s}$) transmission into a set of parallel transmissions with very low data rates ($\frac{1}{NT_s}$). With this structure the problem of high data rate transmission over frequency selective channel has been transformed into a set of simple problems which do not require complicated time domain equalization. Therefore OFDM plays an important role in modern wireless communication where high data rate transmission is commonly required.

2.1 Principles

In OFDM/QAM systems, as shown in Fig. 1, the information bit stream (bit rate $R_b = \frac{1}{T_b}$) is first modulated in baseband using M-QAM modulation (with symbol duration $T_s = T_b \log_2 M$) and then divided into N parallel symbol streams which are multiplied by a pulse shape function $g_{m,n}(t)$. These N parallel signals are then summed and transmitted. On the receiver side, the received signal is first passed through N parallel correlator demodulators (multiplication, integration and sampling) and merged together via parallel-to-serial converter followed by detector and decoder.

The transmitted signal can be written in the following analytic form

$$s(t) = \sum_{n=-\infty}^{+\infty} \sum_{m=0}^{N-1} a_{m,n} g_{m,n}(t) \tag{1}$$

where $a_{m,n} (n \in \mathbb{Z}, m = 0, 1, ..., N-1)$ denotes the baseband modulated information symbol conveyed by the sub-carrier of index m during the symbol time of index n, and $g_{m,n}(t)$ represents the pulse shape of index (m, n) in the synthesis basis which is derived by the time-frequency translated version of the prototype function $g(t)$ in the following

way

$$g_{m,n}(t) \triangleq e^{j2\pi mFt} g(t - nT), \text{ where } m, n \in \mathbb{Z} \tag{2}$$

where $j = \sqrt{-1}$, F represents the inter-carrier frequency spacing and T is the OFDM symbol duration. Therefore $g_{m,n}(t)$ forms an infinite set of pulses spaced at multiples of T and frequency shifted by multiples of F. Consequently the density of OFDM system lattice is

$$\frac{1}{TF}$$

In an OFDM/QAM system, the frequency spacing F is set to $\nu_0 = \dfrac{1}{NT_s}$ and the time shift T is set to τ_0. The prototype function $g(t)$ is defined as follows

$$g(t) = \begin{cases} \frac{1}{\sqrt{\tau_0}}, & 0 \le t < \tau_0 \\ 0, & \text{elsewhere} \end{cases} \tag{3}$$

The orthogonality of the synthesis basis can be demonstrated from the inner product between different elements

$$\begin{aligned} \langle g_{m,n}, g_{m',n'} \rangle &= \int_R g^*_{m,n}(t) g_{m',n'}(t) dt \\ &= \int_R e^{j2\pi(m'-m)\nu_0 t} g^*(t - n\tau_0) g(t - n'\tau_0) dt \\ &= \frac{1}{\sqrt{\tau_0}} \int_{n\tau_0}^{(n+1)\tau_0} e^{j2\pi(m'-m)\nu_0 t} g(t - n'\tau_0) dt \\ &= \delta_{m,m'} \delta_{n,n'} \end{aligned} \tag{4}$$

where the last equality comes from the fact that $\tau_0 \nu_0 = 1$ which is a requirement in OFDM/QAM system, and $\delta_{m,n}$ is the Kronecker delta function defined by

$$\delta_{m,n} = \begin{cases} 1, & m = n \\ 0, & \text{otherwise} \end{cases}$$

.

At the receiver side, the received signal $r(t)$ can be written as

$$r(t) = h * s(t) + n(t) = \sum_{n=-\infty}^{+\infty} \sum_{m=0}^{N-1} h_{m,n} a_{m,n} g_{m,n}(t) + n(t) \tag{5}$$

where h is the wireless channel impulse response and $h_{m,n}$ represents the channel realization on each sub-channel which is assumed to be known by the receiver, $n(t)$ is the additive noise which is usually modeled as AWGN. Passing $r(t)$ through N parallel correlator demodulators with analysis basis which is identical[3] with the synthesis basis defined

[3]not necessary, see OFDM with cyclic prefix in Sec. 2.3

by (2), the output of the l_{th} branch during time interval $n\tau_0 \leq t < (n+1)\tau_0$ is

$$\begin{aligned}\tilde{a}_n(l) = \langle g_{l,n}, r\rangle &= \sum_{k=-\infty}^{+\infty}\sum_{m=0}^{N-1} h_{m,k}a_{m,k}\langle g_{l,n}, g_{m,k}\rangle + \langle g_{l,n}, n\rangle \\ &= \sum_{k=-\infty}^{+\infty}\sum_{m=0}^{N-1} h_{m,k}a_{m,k}\delta_{l,m}\delta_{n,k} + n_n(l) \\ &= \sum_{m=0}^{N-1} h_{m,n}a_{m,n}\delta_{l,m} + n_n(l) \\ &= h_{l,n}a_{l,n} + n_n(l)\end{aligned} \tag{6}$$

In the detector this output is multiplied by a factor $\dfrac{1}{h_{l,n}}$ (nothing but channel inversion) and therefore the transmitted symbol is recovered after demodulation only with presence of AWGN noise.

The spectral efficiency η in this OFDM system can be expressed as

$$\eta = \frac{\beta}{TF} = \frac{\log_2 M}{\tau_0\nu_0} = \log_2 M \text{ [bit/s/Hz]} \tag{7}$$

where $\beta = \log_2 M$ is the number of bits per symbol by M-QAM modulation and $\dfrac{1}{TF} = \dfrac{1}{\tau_0\nu_0} = 1$ is the lattice density of OFDM/QAM system.

2.2 Implementation

If we sample the transmitted signal $s(t)$ at rate $1/T_s$ during time interval $n\tau_0 \leq t < (n+1)\tau_0$ and normalize it by $\sqrt{\tau_0}$, we obtain

$$\begin{aligned}s_n(k) \triangleq s(n\tau_0 + kT_s) &= \sum_{m=0}^{N-1} a_{m,n}e^{j2\pi mFkT_s} \\ &= \sum_{m=0}^{N-1} a_{m,n}e^{j2\pi\frac{mk}{N}}\end{aligned} \quad , \begin{array}{l} k = 0, 1, ..., N-1 \\ n \in \mathbb{Z}\end{array} \tag{8}$$

This sampled transmitted signal $s_n(k)(n \in \mathbb{Z}, k = 0, 1, ..., N-1)$ is the Inverse Discrete Fourier Transform (IDFT)[4] of the modulated baseband symbols $a_{m,n}(n \in \mathbb{Z}, m = 0, 1, ..., N-1)$ during the same time interval. Therefore the OFDM modulator at the transmitter side can be replaced by an IDFT block.

Equivalently, at the receiver side, we sample the received signal $r(t)$ at the same sampling rate $1/T_s$, normalize it by factor $\sqrt{\tau_0}$, and rewrite (6) as follows

$$\tilde{a}_n(l) = \langle g_{l,n}, r\rangle = \int_{n\tau_0}^{(n+1)\tau_0} g_{l,n}^*(t)r(t)dt \simeq \sum_{m=0}^{N-1} r(n\tau_0 + mT_s)e^{-j2\pi\frac{ml}{N}} = \sum_{m=0}^{N-1} r_n(m)e^{-j2\pi\frac{ml}{N}}$$

[4] except for a scaling factor N

The demodulated symbol $\tilde{a}_n(l)(n \in \mathbb{Z}, l = 0, 1, ..., N-1)$ is the Discrete Fourier Transform (DFT) of the received signal $r_n(m)(n \in \mathbb{Z}, m = 0, 1, ..., N-1)$.

Let $\boldsymbol{s}_n = [s_n(0), s_n(1), ..., s_n(N-1)]^T$, $\boldsymbol{a}_n = [a_{0,n}, a_{1,n}, ..., a_{N-1,n}]^T$, $\boldsymbol{r}_n = [r_n(0), r_n(1), ..., r_n(N-1)]^T$, then

$$\begin{aligned} \boldsymbol{s}_n &= \text{IDFT}(\boldsymbol{a}_n) \\ \tilde{\boldsymbol{a}}_n &= \text{DFT}(\boldsymbol{r}_n) \end{aligned}$$

Consequently, the whole system of OFDM/QAM can be efficiently implemented by the FFT/IFFT module and this makes OFDM/QAM an attractive option in high data rate applications.

2.3 Guard Interval and Cyclic Prefix

When there is multipath propagation, consequent OFDM symbols overlap with each other and hence cause serve ISI which degrades the performance of OFDM/QAM system by introducing an error floor for the Bit Error Rate (BER). That is, the BER will converge to a constant value with increasing SNR. A simple and straightforward approach, which is standardized in OFDM applications, is to add a guard interval into the pulse shape function $g(t)$. When the duration of the guard interval T_g is longer than the time dispersion T_d, ISI can be totally removed. With a guard interval added, the prototype function for synthesis basis is as follows

$$q(t) = \begin{cases} \frac{1}{\sqrt{T_0}}, & -T_g \leq t < \tau_0 \\ 0, & \text{elsewhere} \end{cases} \tag{9}$$

where $T_0 = T_g + \tau_0$ is the OFDM symbol duration. Consequently the synthesis basis (2) becomes

$$q_{m,n}(t) = e^{j2\pi m\nu_0 t} q(t - nT_0) \tag{10}$$

On the receiver side the analysis basis prototype function remains the same as defined in (3) with time shift T_0 and integration region $nT_0 \leq t < nT_0 + \tau_0$. The orthogonality condition (4) between synthesis basis and analysis basis therefore becomes

$$\begin{aligned} &\langle g_{m,n}, q_{m',n'} \rangle = \textstyle\int_R e^{j2\pi(m'-m)\nu_0 t} g^*(t - nT_0) q(t - n'T_0) dt \\ &= \tfrac{1}{\sqrt{\tau_0}} \textstyle\int_{nT_0}^{nT_0+\tau_0} e^{j2\pi(m'-m)\nu_0 t} q(t - n'T_0) dt = \begin{cases} \sqrt{\frac{\tau_0}{T_0}}, & m = m' \text{ and } n = n' \\ 0, & \text{otherwise} \end{cases} \end{aligned} \tag{11}$$

Now, assuming that the guard interval $T_g = GT_s, G \in \mathbb{N}$, if we sample the signal $s(t)$ at the same sampling rate $1/T_s$ during the time interval $nT_0 - T_g \leq t < nT_0 + \tau_0$ and normalize it by $\sqrt{T_0}$

$$c_n(k) \triangleq s(nT_0 + kT_s) = \sum_{m=0}^{N-1} a_{m,n} e^{j2\pi \frac{mk}{N}}, \quad \begin{matrix} k = -G, -G+1, ..., 0, ..., N-1 \\ n \in \mathbb{Z} \end{matrix} \tag{12}$$

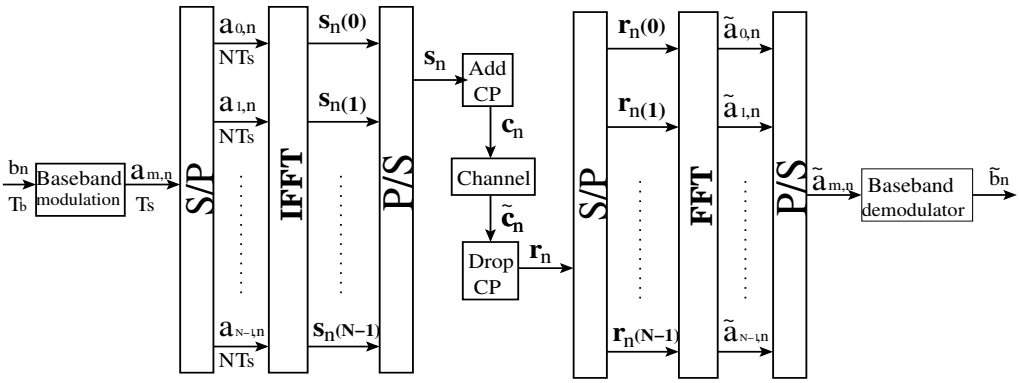

Figure 2: OFDM/QAM system with cyclic prefix.

Rewriting the above expression in vector format, we get

$$\begin{aligned} \boldsymbol{c}_n &= [s_n(-G), s_n(1-G), ..., s_n(-1), s_n(0), ..., s_n(N-1)]^T \\ &= [\underbrace{s_n(N-G), s_n(N-G+1), ..., s_n(N-1)}_{the\ LAST\ G\ elements\ of \boldsymbol{s}_n}, \underbrace{s_n(0), ..., s_n(N-1)}_{\boldsymbol{s}_n}]^T \end{aligned} \tag{13}$$

where the second equality comes from the periodic property of DFT function and the first G elements are referred to as the *Cyclic Prefix* (CP). That is, to add a guard interval into the pulse shape prototype function is equivalent to add a cyclic prefix into the transmitted stream after OFDM modulation (IFFT). At the receiver side, the first G samples which contain ISI are just ignored. The system diagram of OFDM/QAM with cyclic prefix is shown in Fig. 2.

After adding cyclic prefix, the spectral efficiency η in (7) becomes

$$\eta = \frac{\beta}{TF} = \frac{\log_2 M}{(\tau_0 + T_g)\nu_0} = (1 - \frac{T_g}{T_0}) \log_2 M \ \text{[bit/s/Hz]} \tag{14}$$

that is, the cyclic prefix costs a loss of spectral efficiency by $\frac{T_g}{T_0}$.

3 OFDM/OQAM and Pulse Shaping

In the previous section we assumed that the channel is ideal without any frequency offset. Therefore ICI can be made negligible and meanwhile ISI can be successfully removed by adding the cyclic prefix. The wireless channel, however, is far from ideal and a typical channel contains time and frequency dispersion that cause both ISI and ICI due to the lack of orthogonality between the perturbed synthesis basis functions and the analysis basis functions. Furthermore, the cyclic prefix is not for free: It costs increased power consumption and reduces spectral efficiency.

One way to solve this problem is to adopt a proper pulse shape prototype function which is well localized in time and frequency domain so that the combined ISI/ICI can be combated efficiently without utilizing any cyclic prefix. Unfortunately, in Gabor theory the Balian-Low theorem [9] states that, orthogonal basis formed by (2) based on a time

and frequency well localized (compact support) prototype function $g(t)$ does not exist for $TF = 1$. Therefore orthogonal basis and compactly supported pulses cannot be achieved simultaneously for OFDM/QAM systems without guard interval ($TF = \tau_0\nu_0 = 1$). On the other hand, orthogonality which ensures simple demodulation complexity, cannot be given up as it plays an important role in the cost calculation of system applications. This dilemma excludes pulse shaping OFDM/QAM from the candidate list and brings an alternative scheme OFDM/OQAM into sight.

3.1 Principle of OFDM/OQAM

Instead of using complex baseband symbols in OFDM/QAM scheme, real valued symbols modulated by *offset* QAM are transmitted on each sub-carrier with the synthesis basis functions obtained by the time-frequency translated version of this prototype function in the following way

$$g_{m,n}(t) = e^{j(m+n)\pi/2} e^{j2\pi m\nu_0 t} g(t - n\tau_0), \quad \nu_0\tau_0 = 1/2 \tag{15}$$

To maintain the orthogonality among the synthesis and analysis basis, modified inner product is defined as follows

$$\langle x, y \rangle_{\mathbb{R}} = \Re \left\{ \int_{\mathbb{R}} x^*(t) y(t) dt \right\}$$

where $\Re\{\bullet\}$ is the real part operator. That is, only the real part of the correlation function is taken into consideration. Consequently, the inner product (cross correlation) between $g_{m,n}(t)$ and $g_{m',n'}(t)$ becomes

$$\begin{aligned}
&\langle g_{m,n}, g_{m',n'} \rangle_{\mathbb{R}} = \Re \left\{ \int_{\mathbb{R}} e^{j(m'+n'-m-n)\pi/2} e^{j2\pi(m'-m)\nu_0 t} g(t - n'\tau_0) g^*(t - n\tau_0) dt \right\} \\
&= \Re \left\{ e^{j\frac{\pi}{2}(m'-m+n'-n+(m'-m)(n+n')2\nu_0\tau_0)} \int_{\mathbb{R}} e^{j2\pi(m'-m)\nu_0 x} g(x + \frac{n-n'}{2}\tau_0) g^*(x - \frac{n-n'}{2}\tau_0) dx \right\} \\
&= \Re \left\{ (j)^{m'-m+n'-n+(m'-m)(n+n')} \int_{\mathbb{R}} e^{-j2\pi(m-m')\nu_0 x} g(x + \frac{n-n'}{2}\tau_0) g^*(x - \frac{n-n'}{2}\tau_0) dx \right\} \\
&= \Re \left\{ (j)^{m'-m+n'-n+(m'-m)(n+n')} A_g((n-n')\tau_0, (m-m')\nu_0) \right\}
\end{aligned} \tag{16}$$

where the second equality comes from variable substitution $t = x + \frac{(n+n')\tau_0}{2}$ and the third equality comes from the fact that $\nu_0\tau_0 = \frac{1}{2}$. $A_g(\tau, \nu)$ is the well known (auto-)ambiguity function (see also Sec. 4.1.2) which is defined as

$$A_g(\tau, \nu) = \int_{\mathbb{R}} \gamma_g(\tau, t) e^{-j2\pi\nu t} dt = \int_{\mathbb{R}} e^{-j2\pi\nu t} g(t + \tau/2) g^*(t - \tau/2) dt \tag{17}$$

where the instantaneous[5] auto-correlation function $\gamma_g(\tau, t) = g(t+\tau/2)g^*(t-\tau/2)$ is even conjugate[6] along the t axis as long as $g(t)$ is an even function. Therefore its Fourier

[5] "instantaneous" is used here to indicate that no expectation is taken compared to the common correlation function.

[6] $\gamma_g(\tau, t) = \gamma_g^*(\tau, -t)$, see (37)

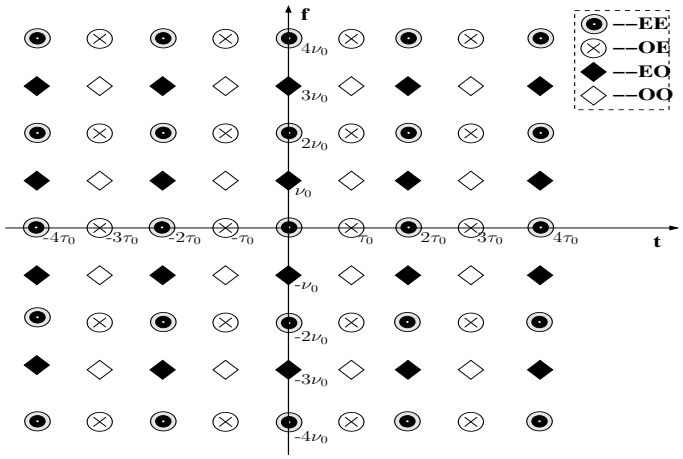

Figure 3: OFDM/OQAM Lattice.

Transform $A_g(\tau,\nu)$ is a real valued function and (16) can be rewritten as

$$\langle g_{m,n}, g_{m',n'}\rangle_{\mathbb{R}} = \begin{cases} \pm A_g((n-n')\tau_0,(m-m')\nu_0) & ,(m,n)=(m',n') \bmod 2 \\ 0 & ,(m,n)\neq(m',n') \bmod 2 \end{cases} \tag{18}$$

By grouping the basis $g_{m,n}(t)$ which satisfies $(m,n)=(m',n') \bmod 2$ into the same subset, the corresponding system lattice $g_{m,n}$ in the time-frequency plane can be decomposed into four sub-lattices: **EE**=$\{m$ even, n even$\}$, **EO**=$\{m$ even, n odd$\}$, **OE**=$\{m$ odd, n even$\}$ and **OO**=$\{m$ odd, n odd$\}$ [11], as shown in Fig. 3.

Whenever $g_{m,n}(t)$ and $g_{m',n'}(t)$ belong to different sub-lattices, the orthogonality is automatically maintained and is independent of the prototype function as long as this function is even. While inside the same sub-lattice, the orthogonality only depends on the ambiguity function $A_g(\tau,\nu)$ and hence can be ensured by just finding an even prototype function whose ambiguity function satisfies

$$A_g(2p\tau_0,2q\nu_0) = \begin{cases} 1, & \text{when } (p,q)=(0,0) \\ 0, & \text{when } (p,q)\neq(0,0) \end{cases} \quad \text{where } p,q\in\mathbb{Z} \tag{19}$$

At the receiver side

$$\begin{aligned} \tilde{a}_n(l) &= \langle g_{l,n}, r\rangle_{\mathbb{R}} = \sum_{k=-\infty}^{+\infty}\sum_{m=0}^{N-1} h_{m,k}a_{m,k}\langle g_{l,n}, g_{m,k}\rangle_{\mathbb{R}} + \langle g_{l,n}, n\rangle_{\mathbb{R}} \\ &= \sum_{m=0}^{N-1} h_{m,n}a_{m,n}\langle g_{l,n}, g_{m,n}\rangle_{\mathbb{R}} + n_n(l) \\ &= h_{l,n}a_{l,n} + n_n(l) \end{aligned}$$

where $h_{l,n}$ is the amplitude of the channel realization which is assumed known by the receiver.

Fig. 3 can also be used for comparison of spectral density between OFDM/QAM ($\tau_0=\nu_0=1$) and OFDM/OQAM ($\tau_0\nu_0=\frac{1}{2}$) systems. Assuming in the OFDM/OQAM system

$\nu_0 = 1$, $\tau_0 = \frac{1}{2}$ for convenience, then the OFDM/QAM system transmits complex symbols on these black solid lattice points (**EE**, **EO**) while the OFDM/OQAM system transmit the real parts of complex symbols on these black solid lattice points and the imaginary parts on these white hollow lattice points (**OE**, **OO**). Therefore the OFDM/OQAM system has doubling symbol rate but half coding rate compared with the OFDM/QAM system, which results in the same data rate per frequency usage and per time unit (spectral efficiency).

So far, two things have to be noted:

- On system level, OFDM/OQAM has twice the system lattice density (for $g_{m,n}$, $\frac{1}{\tau_0\nu_0} = 2$) but half the coding rate (only transmit real-valued symbols) compared to OFDM/QAM without cyclic prefix, therefore it has the same spectral efficiency ($\eta = \frac{1/2\log_2 M}{\tau_0\nu_0} = \log_2 M$ [bit/s/Hz]), as OFDM without cyclic prefix, cf. (7).
- For prototype function design, OFDM/OQAM has less lattice density requirement ($A_g(\tau,\nu) = 0 \Rightarrow \frac{1}{2\tau_0 2\nu_0} = \frac{1}{2}$) compared to OFDM/QAM ($\frac{1}{\tau_0\nu_0} = 1$).

The above two features make it possible for OFDM/OQAM system to find a well-localized prototype function while maintaining (bi-)orthogonality and therefore makes pulse shaping OFDM/OQAM an attractive candidate for a time frequency dispersive channel.

3.2 Pulse Shaping

The idea of pulse shaping OFDM/OQAM is to find an efficient transmitter and a corresponding receiver waveform for the current channel condition [3][13]. Specifically, a *good* signal waveform should be compactly supported and well localized in time and in frequency with the same time-frequency scale as the channel itself:

$$\frac{\tau_0}{\Delta\tau} = \frac{\nu_0}{\Delta\nu}$$

where $\Delta\tau$ and $\Delta\nu$ is the rms (root-mean-square) delay spread and frequency (Doppler) spread[7] of the wireless channel, respectively.

For example, in indoor situations the time dispersion is usually small, see Fig 4, a vertically stretched time-frequency pulse is suitable and where the frequency dispersion is small, a horizontally stretched pulse is suitable. This enables a very efficient packing [17] of time-frequency symbols and hence maximizes e.g. the throughput or the interference robustness in the communication link. In the following part of this section, several different types of pulse shape functions are presented, namely the rectangular function, the half cosine function, the Gaussian function, the IOTA function and the EFG.

3.2.1 Rectangular Function

The rectangular prototype function is a possible choice and can be a benchmark for comparison. A time shift has to be applied to ensure the even function property, as

[7] for discrete channel model, the maximum delay and Doppler spread will be used instead.

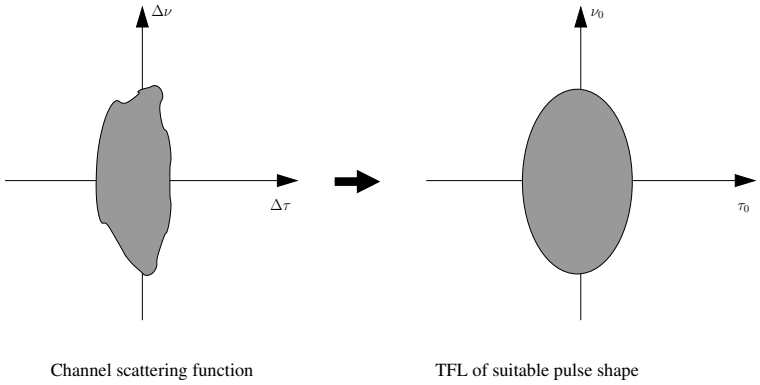

Figure 4: Channel scattering function and corresponding pulse shape.

shown in (20).

$$g(t) = \begin{cases} \frac{1}{\sqrt{\tau_0}}, & |t| \leq \frac{\tau_0}{2} \\ 0, & \text{elsewhere} \end{cases} \tag{20}$$

By interchanging time and frequency axes, the dual of the rectangular function becomes a natural extension, which is defined in the frequency domain as follows

$$G(f) = \begin{cases} \frac{1}{\sqrt{\nu_0}}, & |f| \leq \frac{\nu_0}{2} \\ 0, & \text{elsewhere} \end{cases} \tag{21}$$

with its inverse Fourier transform

$$g(t) = \frac{\sin(\pi\nu_0 t)}{\pi t\sqrt{\nu_0}}$$

This function is nothing but a sampling interpolation function. Its obvious advantage over rectangular function is that there is no overlapping in the frequency domain and therefore causes less interference. On the other hand, with a longer duration in the time domain, the implementation and equalization complexity is considerable even after proper truncation.

3.2.2 Half Cosine Function

A conventional prototype function in OFDM/OQAM system is the half cosine function which is defined by

$$g(t) = \begin{cases} \frac{1}{\sqrt{\tau_0}} \cos\frac{\pi t}{2\tau_0}, & |t| \leq \tau_0 \\ 0, & \text{elsewhere} \end{cases} \tag{22}$$

It has a compact support[8] in the time domain and meanwhile a fast decay in the frequency domain, as shown in Fig. 5, and therefore serves as a good prototype function.

[8]A function $x(t)$ is said to be compact support if there exists a constant $\sigma > 0$ so that $x(t) = 0$ for all $|x| > \sigma$.

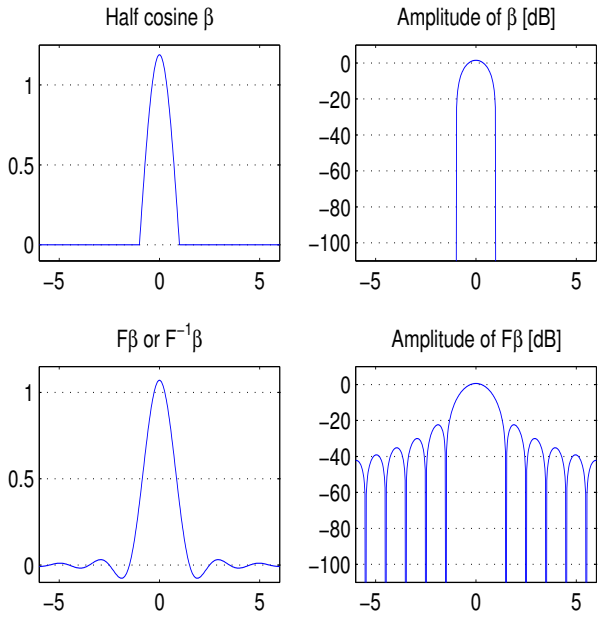

Figure 5: Half cosine function and its Fourier transform.

Similarly, its dual form is instead defined by its Fourier transform as

$$G(f) = \begin{cases} \frac{1}{\sqrt{\nu_0}} \cos \frac{\pi f}{2\nu_0}, & |f| \leq \nu_0 \\ 0, & \text{elsewhere} \end{cases} \tag{23}$$

This prototype function can be extended to any real even function whose Fourier transform $G(f)$ satisfies the following conditions:

$$\begin{cases} |G(f)|^2 + |G(f-\nu_0)|^2 = 1/\nu_0 & |f| \leq \nu_0 \\ G(f) = 0 & \text{otherwise} \end{cases} \tag{24}$$

which corresponds to a half-Nyquist filter [1].

3.2.3 Gaussian Function

Gaussian function is very famous for that its Fourier transform has maintains the same shape as itself except for an axis scaling factor. For a Gaussian function

$$g_\alpha(t) = (2\alpha)^{1/4} e^{-\pi\alpha t^2}, \ \alpha > 0 \tag{25}$$

its Fourier transform is

$$\begin{aligned} \mathcal{F} g_\alpha(t) &= (2\alpha)^{1/4} \int_{-\infty}^{\infty} e^{-\pi\alpha t^2} e^{-j2\pi f t} dt = (2\alpha)^{1/4} \sqrt{\frac{\pi}{\pi\alpha}} e^{(-j\pi f)^2/(\pi\alpha)} \\ &= (2/\alpha)^{1/4} e^{-\pi f^2/\alpha} = g_{1/\alpha}(f). \end{aligned} \tag{26}$$

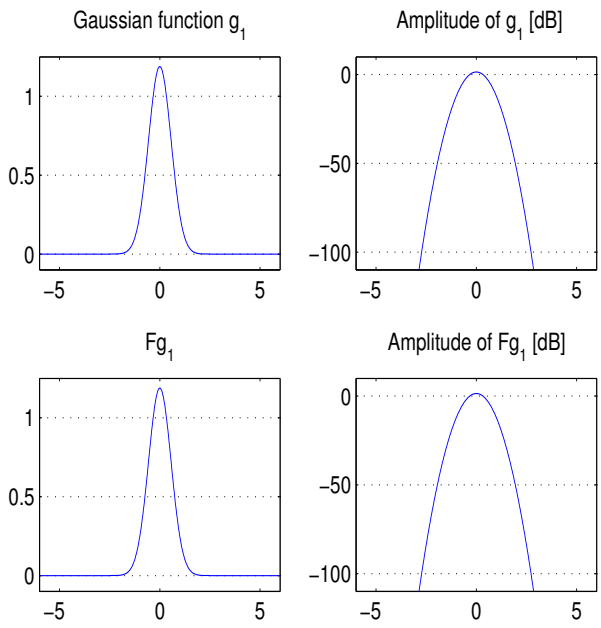

Figure 6: Gaussian function with $\alpha = 1$ and its Fourier transform.

Here the second equality comes from the fact that [10]

$$\int_{-\infty}^{\infty} e^{2bt-at^2} dt = \sqrt{\frac{\pi}{a}} e^{b^2/a} \ (a > 0)$$

As the Gaussian prototype function is perfectly isotropic (invariant under rotation) and has fast decay both in time and frequency domain, as shown in Fig. 6, it seems to be an attractive candidate for pulse shaping prototype function. On the other hand, the basis function generated by Gaussian prototype function is in no way orthogonal as $g_\alpha(t) > 0$ holds on the whole real axis. Therefore the Gaussian function is not considered here.

3.2.4 Isotropic Orthogonal Transform Algorithm (IOTA) Function

Orthogonality between basis functions is normally obtained by using either a time or frequency limitation of the prototype function, for example, the rectangular function and the half cosine function. A different approach, called Isotropic Orthogonal Transform Algorithm (IOTA), is presented in [1, 11] and summarized bellow.

Define $\mathcal{O}_a$ as the orthogonalization operator on function $x(t)$ according to the following relation

$$\mathcal{O}_a x = \frac{x(t)}{\sqrt{a \sum_{k=-\infty}^{\infty} |x(t-ka)|^2}}, \ a > 0 \tag{27}$$

The effect of the operator $\mathcal{O}_a$ is to orthogonalize the function $x(t)$ along the frequency axis, which can be seen directly on the ambiguity function

$$A_y(0, \frac{m}{a}) = 0, \ \forall m \neq 0 \text{ and } A_y(0,0) = 1 \tag{28}$$

where $y(t) = \mathcal{O}_a x(t)$. That is, the resulting function $y(t)$ and its frequency shifted versions construct an orthonormal set of functions. The proof can be found in Appendix A.

Similarly, in order to orthogonalize $x(t)$ along the time axis, one can turn to frequency domain and apply this orthogonalization operator to $X(f)$,which is the Fourier transform of $x(t)$. To carry out this operation on $x(t)$, one has first to transfer it into frequency domain by Fourier transform $\mathcal{F}$, then apply to the orthogonalization operation $\mathcal{O}_a$, and then go back to the time domain by inverse Fourier transform $\mathcal{F}^{-1}$. For $y(t) = \mathcal{F}^{-1}\mathcal{O}_a\mathcal{F}x(t)$, we have

$$A_y(\frac{n}{a}, 0) = 0, \ \forall n \neq 0 \text{ and } A_y(0,0) = 1 \tag{29}$$

Hence the resulting function and its time delayed forms are orthonormal.

Starting from the Gaussian function $g_\alpha(t)$, by applying $\mathcal{O}_{\tau_0}$ we get $y_\alpha(t) = \mathcal{O}_{\tau_0} g_\alpha(t)$ and

$$A_y(0, \frac{m}{\tau_0}) = 0, \ \forall m \neq 0, \text{ and } A_y(0,0) = 1$$

which comes from (28) and shows that y_α is orthogonal to its frequency shifted copies at multiples of $\frac{m}{\tau_0}$. Then apply $\mathcal{F}^{-1}\mathcal{O}_\nu\mathcal{F}$ to $y_\alpha(t)$, we get

$$z_{\alpha,\nu_0,\tau_0}(t) = \mathcal{F}^{-1}\mathcal{O}_{\nu_0}\mathcal{F}y_\alpha(t) = \mathcal{F}^{-1}\mathcal{O}_{\nu_0}\mathcal{F}\mathcal{O}_{\tau_0}g_\alpha(t) \overset{[11]}{=} \mathcal{O}_{\tau_0}\mathcal{F}^{-1}\mathcal{O}_{\nu_0}\mathcal{F}g_\alpha(t) \tag{30}$$

and

$$A_z(\frac{n}{\nu_0}, \frac{m}{\tau_0}) = A_z(2n\tau_0, 2m\nu_0) = 0, \ (m,n) \neq (0,0) \tag{31}$$

where the first equality comes from the fact that $\tau_0\nu_0 = \frac{1}{2}$ and the second equality is the straightforward result of time and frequency orthogonalization. Therefore, the requirement in (19) is automatically satisfied as normalization is embedded in the above process of orthogonalization.

As $y_\alpha = \mathcal{O}_{\tau_0} g_\alpha$ is even, $\mathcal{F}y_\alpha = \mathcal{F}^{-1}y_\alpha$. Recall the Fourier transform invariant property of Gaussian displayed in (26), and apply it to z_{α,ν_0,τ_0}

$$\begin{aligned} \mathcal{F}z_{\alpha,\nu_0,\tau_0} &= \mathcal{F}\mathcal{F}^{-1}\mathcal{O}_{\nu_0}\mathcal{F}y_\alpha = \mathcal{O}_{\nu_0}\mathcal{F}y_\alpha = \mathcal{O}_{\nu_0}\mathcal{F}^{-1}y_\alpha \\ &= \mathcal{O}_{\nu_0}\mathcal{F}^{-1}\mathcal{O}_{\tau_0}g_\alpha = \mathcal{O}_{\nu_0}\mathcal{F}^{-1}\mathcal{O}_{\tau_0}\mathcal{F}g_{1/\alpha} = z_{1/\alpha,\tau_0,\nu_0} \end{aligned} \tag{32}$$

Let $\alpha = 1$, $\tau_0 = \nu_0 = \frac{1}{\sqrt{2}}$ and define $\zeta(t) = z_{1,\frac{1}{\sqrt{2}},\frac{1}{\sqrt{2}}}(t)$, then we have

$$\mathcal{F}\zeta = \mathcal{F}z_{1,\frac{1}{\sqrt{2}},\frac{1}{\sqrt{2}}} = z_{1,\frac{1}{\sqrt{2}},\frac{1}{\sqrt{2}}} = \zeta \tag{33}$$

Thus ζ is identical to its Fourier transform, as shown in Fig. 7, and has nearly isotropic support over the whole time-frequency plane. This is the reason why it is named IOTA function.

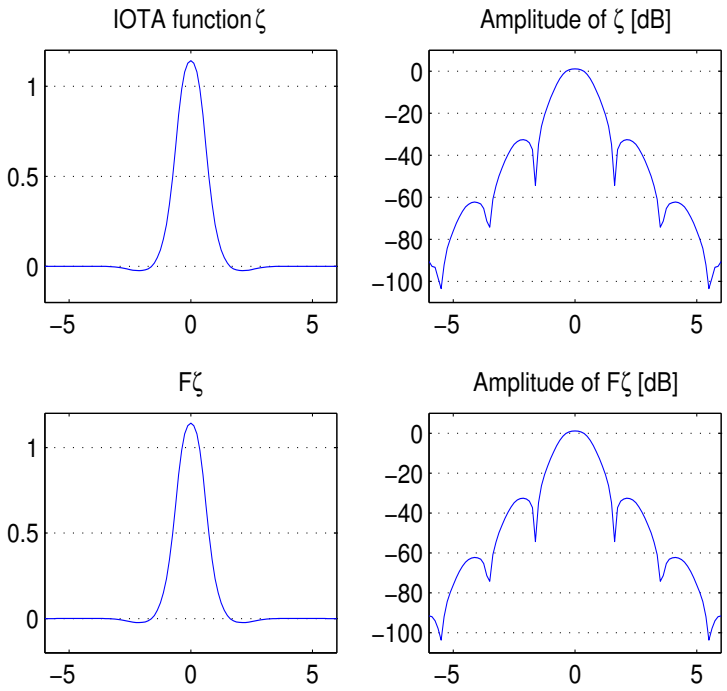

Figure 7: IOTA function and its Fourier transform.

3.2.5 Extended Gaussian Function (EGF)

It is shown [11, 12] that the function z_{α,ν_0,τ_0} which is generated by the algorithmic approach described in (30) has a closed-form analytical expression[9]

$$z_{\alpha,\nu_0,\tau_0}(t) = \frac{1}{2}\left[\sum_{k=0}^{\infty} d_{k,\alpha,\nu_0}\left[g_\alpha(t+\frac{k}{\nu_0}) + g_\alpha(t-\frac{k}{\nu_0})\right]\right]\sum_{l=0}^{\infty} d_{l,1/\alpha,\tau_0}\cos(2\pi l\frac{t}{\tau_0}) \qquad (34)$$

where $\tau_0\nu_0 = \frac{1}{2}$, $0.528\nu_0^2 \leq \alpha \leq 7.568\nu_0^2$, g_α is the Gaussian function, and the coefficients d_{k,α,ν_0} are real valued and can be computed via the rules described in [11, 12], c.f. Appendix B. This family of functions are named as Extended Gaussian Function (EGF) as they are derived from the Gaussian function. The IOTA function ζ is therefore a special case of EGF and its properties such as orthogonality and good time frequency localization are shared with these EGF functions.

In practice, as reported in [11], the infinite summation in EGF can be truncated to fifty or even fewer terms while keeping excellent orthogonality and TFL. An approximation of EGF with a few terms is also possible while the trade-off between localization and orthogonality has to be sought.

3.3 Implementation

As shown in Sec. 2, the OFDM/QAM system can be efficiently implemented by FFT/IFFT modules, whereas in an OFDM/OQAM system the envelope of the prototype function is

[9] A general expression with $\tau_0\nu_0 = \frac{1}{2n}$, $n \in \mathbb{N}$ is omitted since $N > 1$ is not interesting for practical usage due to higher lattice density requirement.

not constant and therefore needs filters to do pulse shaping. A direct implementation of the OFDM/OQAM system with finite impulse response (FIR) filters on each sub-carrier branch will be time consuming and cause a large delay. As the duration of the even prototype function can be very long (e.g. IOTA and EGF is theoretically infinite), a large delay has to be introduced to make the system causal (i.e., realizable[10]). Alternatively, another approach which utilizes filter banks combined with FFT/IFFT blocks [12, 14] provides a very efficient implementation and preserves the orthogonality of the prototype functions.

4 Orthogonality and Time Frequency Localization (TFL)

Orthogonal basis is preferred in the design of digital communication systems as it simplifies the reconstruction of the transmitted signal and provides a ISI/ICI-free scheme in AWGN channel. On the other hand, as mentioned in Sec. 3, the wireless channel is doubly dispersive and therefore requires pulse shapes with good time frequency localization (TFL). A prototype function with nearly compact support on the time-frequency plane will ensure good ISI/ICI robustness but degrade the orthogonality, if the same time-frequency lattice density ($\frac{1}{TF}$) is required. The IOTA function, which is orthogonal and well localized, actually comes from halving lattice density ($\frac{1}{TF} = \frac{1}{2\tau_0 2\nu_0} = \frac{1}{2}$, also see equations (19) and (31)). Therefore, a trade off between orthogonality and TFL must be sought according to the channel realization so that maximum spectral density (or throughput) can be reached at the targeted BER.

4.1 Time Frequency Localization

The time-frequency translated versions of the prototype function, as shown in equations (2, 10, 15), form a lattice in the time-frequency plane. If the prototype function, which is assumed to be centered around the origin, has nearly compact support over the time-frequency plane, the transmitted signal composed by these basis functions will place a copy of the prototype function on each lattice point in the time-frequency plane and therefore illustrate from this intuitive image how the signal from different carriers and different symbols get along with one other. The less power the prototype function spreads to the neighboring lattice region, the better reconstruction of the transmitted signal can be retrieved after demodulation.

Several functions, the instantaneous correlation function, the ambiguity function and the interference function, are commonly used to demonstrate the TFL property and are therefore discussed bellow.

4.1.1 Instantaneous Correlation Function

Two kinds of instantaneous correlation functions is usually used: the instantaneous cross-correlation function and the instantaneous autocorrelation function. The instantaneous

[10] A system is realizable if and only if it is causal.

cross-correlation function between synthesis prototype function $g(t)$ and analysis prototype function $q(t)$ is defined as

$$\gamma_{g,q}(\tau,t) = g(t+\tau/2)q^*(t-\tau/2) \tag{35}$$

and the instantaneous auto-correlation function is as follows

$$\gamma_g(\tau,t) \triangleq \gamma_{g,g}(\tau,t) = g(t+\tau/2)g^*(t-\tau/2) \tag{36}$$

When $g(t)$ is even, we get

$$\gamma_g^*(\tau,-t) = g^*(-t+\tau/2)g(-t-\tau/2) = g^*(t-\tau/2)g(t+\tau/2) = \gamma_g(\tau,t) \tag{37}$$

which states that $\gamma_g(\tau,t)$ is even conjugate.

4.1.2 Ambiguity Function

Recall the definition of ambiguity function in (17),which is defined as the Fourier transform of the instantaneous correlation function along the time axis t, the corresponding cross-ambiguity function between $g(t)$ and $q(t)$ is

$$\begin{aligned} A_{g,q}(\tau,\nu) &\triangleq \int_{\mathbb{R}} \gamma_{g,q}(\tau,t)e^{-j2\pi\nu t}dt = \int_{\mathbb{R}} g(t+\tau/2)q^*(t-\tau/2)e^{-j2\pi\nu t}dt \\ &= e^{-j\pi\tau\nu}\int_{\mathbb{R}} g(t+\tau)q^*(t)e^{-j2\pi\nu t}dt = e^{-j\pi\tau\nu} < q(t)e^{j2\pi\nu t}, g(t+\tau) > \end{aligned} \tag{38}$$

where the similar variable substitution is exploited as in (16). Similarly, the auto-ambiguity function which is the same as in (17), can be regarded as a special case of the cross-ambiguity function when $g(t) = q(t)$

$$A_g(\tau,\nu) \triangleq \int_{\mathbb{R}} \gamma_g(\tau,t)e^{-j2\pi\nu t}dt = e^{-j\pi\tau\nu} < g(t)e^{j2\pi\nu t}, g(t+\tau) > \tag{39}$$

As long as the prototype function is normalized (i.e. unity energy), the maximum of the auto-ambiguity function is

$$\max_{\tau,\nu} |A_g(\tau,\nu)| = A_g(0,0) = 1$$

On the other hand, the maximum value of the cross-ambiguity function $\max_{\tau,\nu} |A_{g,q}(\tau,\nu)|$ depends on the matching between $g(t)$ and $q(t)$ and hence is equal to or less than unity. The ambiguity function can therefore be used as an indicator of the orthogonality/similarity between the prototype function and its time and frequency translated version (e.g. $|A_g(\tau,\nu)| = 0$ means *orthogonal* and $|A_g(\tau,\nu)| = 1$ means *identical*), or to show to what an extent the synthesis basis is matched to the corresponding analysis basis (the larger $|A_{g,q}(\tau,\nu)|$ is, the better the demodulator works).

According to (16) and (18), also indicated in Fig. 3, only the basis functions that belong to the same sub-lattice can remain after demodulation by the real inner product. Take the channel time and frequency spread into account, the ambiguity function can

be used to shown how this spread will affect the demodulation gain. Let's only consider the origin point in the TFL plane and its neighboring points in the same sub-lattice, i.e. $g_{m,n},\ m,n \in \{-2,0,2\}$, with time spread τ and frequency spread ν added to channel realization, the output of demodulator is

$$\begin{aligned}
\langle g(t), r'(t)\rangle_{\mathbb{R}} &= \left\langle g(t), \sum_{m,n\in\{-2,0,2\}} h_{m,n}a_{m,n}e^{j\frac{\pi}{2}(m+n)}g(t-n\tau_0+\tau)e^{j2\pi(m\nu_0-\nu)t}\right\rangle_{\mathbb{R}} \\
&= \sum_{m,n\in\{-2,0,2\}} h_{m,n}a_{m,n}\,\Re\left\{e^{j\frac{\pi}{2}(m+n)}\int_{\mathbb{R}} g(t+\tau-n\tau_0)g^*(t)\,e^{-j2\pi(\nu-m\nu_0)t}dt\right\} \\
&= \sum_{m,n\in\{-2,0,2\}} \Re\left\{e^{j\frac{\pi}{2}(m+n)}e^{j\pi(\tau-n\tau_0)(\nu-m\nu_0)}h_{m,n}a_{m,n}A_g(\tau-n\tau_0,\nu-m\nu_0)\right\} \\
&= \sum_{m,n\in\{-2,0,2\}} \Re\left\{e^{j\frac{\pi}{2}(m+n)}e^{j\pi(\tau-n\tau_0)(\nu-m\nu_0)}\right\}h_{m,n}a_{m,n}A_g(\tau-n\tau_0,\nu-m\nu_0)
\end{aligned} \tag{40}$$

where the third equality comes from (39) and the last equality comes from the fact that $A_g(\tau,\nu)$ is real as for even prototype functions. Therefore, the maximum demodulation gain is determined by the ambiguity function and affected by the channel time and frequency dispersion. A three dimensional plot will be presented later to show this point clearly.

Several important features of the ambiguity function need to be highlighted:

- It is a two dimensional (auto-)correlation function in the time-frequency plane.
- It is real valued in the case of an even prototype function, i.e. $g(-t) = g(t)$.
- It illustrates the sensitivity to delay and frequency offset.
- It gives an intuitive demonstration of ICI/ISI robustness.

4.1.3 Interference Function

To obtain a more clear image of how much interference (power) has been induced to other symbols on the time frequency lattice, a so called interference function has been introduced

$$I(\tau,\nu) = 1 - |A(\tau,\nu)|^2 \tag{41}$$

where $A(\tau,\nu) = A_g(\tau,\nu)$ in an OFDM/QAM system and $A(\tau,\nu) = \Re[A_g(\tau,\nu)]$ in an OFDM/OQAM system for the auto-ambiguity function case. In the case of cross-ambiguity function, $A(\tau,\nu) = A_{g,q}(\tau,\nu)$ has to be normalized so that $I(\tau,\nu) = 0$ when there is no interference.

4.2 Heisenberg Parameter ξ

Let $x(t)$ be a function with Fourier transform $X(f)$, and choose the Heisenberg parameter [1, 11], which is derived from the Heisenberg Uncertainty Principle [9], to measure the TFL property, which is given by

$$\xi = \frac{1}{4\pi\Delta t\Delta f} \leq 1 \tag{42}$$

where Δt is the mass moment of inertia of the prototype function in time and Δf in frequency, which shows how the energy (mass) of the prototype function spreads over the time and frequency plane. The larger Δt (Δf), the more spread there is concerning the time (frequency) support of the prototype function. These two parameters can be calculated via the following set of equations

$$\begin{cases} \Delta t^2 &= \frac{1}{E}\int_{\mathbb{R}}(t-\bar{t})^2|x(t)|^2dt \\ \Delta f^2 &= \frac{1}{E}\int_{\mathbb{R}}(f-\bar{f})^2|X(f)|^2df \\ \bar{t} &= \frac{1}{E}\int_{\mathbb{R}} t|x(t)|^2dt \\ \bar{f} &= \frac{1}{E}\int_{\mathbb{R}} f|X(f)|^2df \\ E &= \int_{\mathbb{R}}|x(t)|^2dt = \int_{\mathbb{R}}|X(f)|^2df \end{cases} \tag{43}$$

where E is the energy of the prototype function, $\bar{t}$ and $\bar{f}$ are the center value (center of gravity) of the time and frequency energy distribution and corresponding to the coordinates of its lattice point in the time-frequency plane, i.e., for $x(t) = g_{m,n}(t)$, it is easy to prove that $\bar{t} = n\tau_0$ and $\bar{f} = m\nu_0$. Therefore, $(\bar{t}, \bar{f})$ indicates the center position in the time-frequency plane of the prototype function and $(\Delta t, \Delta f)$ describes how large area it occupies to accommodate most of its energy.

According to the Heisenberg uncertainty inequality, $0 \leq \xi \leq 1$, where the upper bound $\xi = 1$ is achieved by the Gaussian function and the lower band $\xi = 0$ is achieved by the rectangular function whose Δf is infinite. The larger ξ is, the better joint time-frequency localization the prototype function has (or alternatively speaking, the less area it occupies). Although the Gaussian function enjoys he minimum joint time-frequency localization (highest TFL parameter), it is not orthogonal as stated before.

5 Numerical Results

Simulations regarding the orthogonality and TFL properties of different prototype functions are carried out in Matlab. For each prototype function, its instantaneous correlation function, ambiguity function, and the corresponding interference function are plotted as three dimensional figures as well as two dimensional contour plots, which are shown in the following. As the rectangular prototype function appears both in OFDM/QAM and OFDM/OQAM systems, although the center and duration is not the same, its main properties regarding orthogonality and TFL are similar. Therefore we just demonstrate the result of OFDM/QAM system, where the rectangular function is time shifted to ensure the symmetry around origin for comparison with the prototype functions in OFDM/OQAM system.

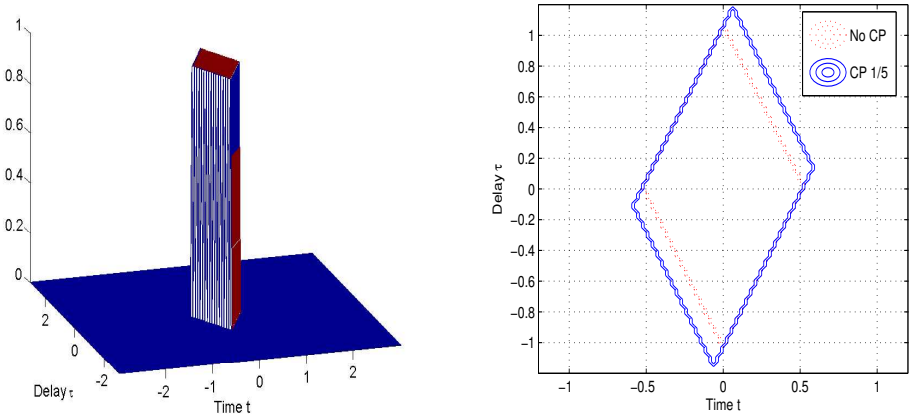

(a) correlation function (b) contour plots

Figure 8: Rectangular prototype for cases of no-CP (dot) and CP (solid) with ($\frac{T_g}{T_0} = \frac{1}{5}$).

5.1 OFDM/QAM and Cyclic Prefix

For OFDM/QAM with a rectangular prototype function, these simulation parameters are set as bellow:

- Time and frequency shift: $\tau_0 = 1$, $\nu_0 = 1$
- Symbol duration: $T_0 = \tau_0$ for no-CP and $T_0 = 1.25\tau_0$ for CP case
- Observation window length: 12 time and frequency shifts, i.e., $t \in [-6\tau_0, 6\tau_0]$ and $f \in [-6\nu_0, 6\nu_0]$
- Samples per time and frequency shift: 32
- Cyclic prefix: No-CP and CP with $\frac{T_g}{T_0} = \frac{0.25}{1.25} = \frac{1}{5}$
- Figures: axes normalized by τ_0 and ν_0 respectively

For OFDM/QAM without cyclic prefix, auto-correlation function (36), auto-ambiguity function (39) are used to get these figures. For OFDM/QAM with cyclic prefix, (35) and (38) are used instead. Plots for interference function are obtained via (41) with attention paid to proper normalization for the cyclic prefix case.

Fig. 8 shows how the correlation function of rectangular prototype function looks like and demonstrates the difference between OFDM/QAM systems with and without cyclic prefix. The Sharp edge of the correlation function comes from the time limitation of the rectangular function. Compared to no-CP case, cyclic prefix enlarges the coverage of the correlation function and reduces the sensitivity to time spread. This "extra" coverage can easily be found at the upper-right border and lower-left border of the contour plots shown in Fig. 8(b).

Fig. 9 displays the ambiguity function which demonstrates how the mismatch in time and frequency between the analysis basis and the corresponding synthesis basis will affect

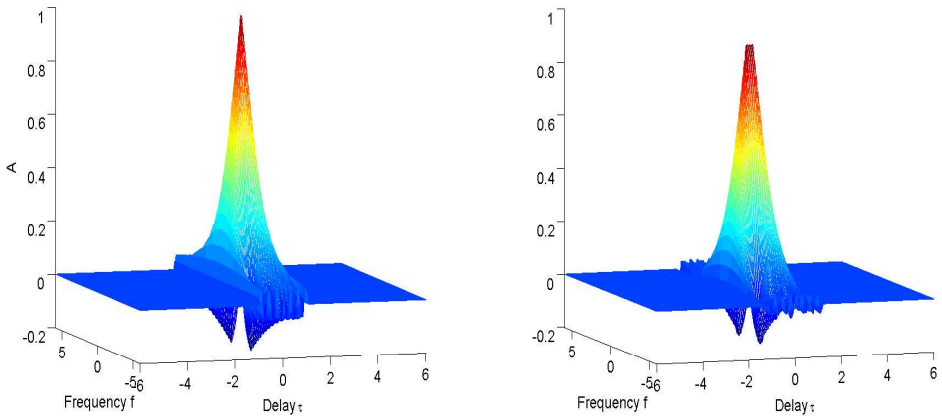

(a) No cyclic prefix (b) Cyclic prefix $\frac{T_g}{T_0} = \frac{1}{5}$

Figure 9: Ambiguity function of rectangular prototype.

the demodulation, or equivalently, how large the power leakage of the prototype function is between neighboring lattice points after time and frequency dispersion being added by the channel, where the role the cyclic prefix plays is clearly shown. In on-CP case shown in Fig. 9(a), the demodulation gain will fall sharply even with a minor time or frequency mismatch. After cyclic prefix is added, as shown in Fig. 9(b), the demodulation gain will remain the same as long as the time mismatch is within the length of cyclic prefix duration. This property is shown more clear by their contour plots.

In no-CP case shown by the contour plots in Fig. 10(a), as long as the time distance between neighboring OFDM symbols larger than τ_0 (i.e., larger than 1 in time axis normalized by τ_0), there is no interference between subsequent OFDM symbols. As there is always power leakage between different sub-carriers in the same time interval, this OFDM/QAM system has a very high sensitivity to frequency offset, which is well known. This has not been intuitively shown until the ambiguity function is used to demonstrate the TFL property. As the contour plots provide a clearer image of the quantity aspects, it will be the main tool to display the comparison between different schemes.

The sensitivity of OFDM/QAM system to time and frequency spread and the effect of cyclic prefix have been intuitively demonstrated by the interference function plotted in Fig. 11 and Fig. 12. The width of the flat bottom of the interference function for cyclic prefix corresponds to the length of the cyclic prefix added into the synthesis basis functions.

5.2 Pulse Shaping OFDM/OQAM

Similar to OFDM/QAM system, the OFDM/OQAM with different prototype functions has its simulation parameters set as following:

- Time and frequency shift: $\tau_0 = \nu_0 = \frac{1}{\sqrt{2}}$ for simplicity
- Symbol duration: $T_0 = \tau_0$

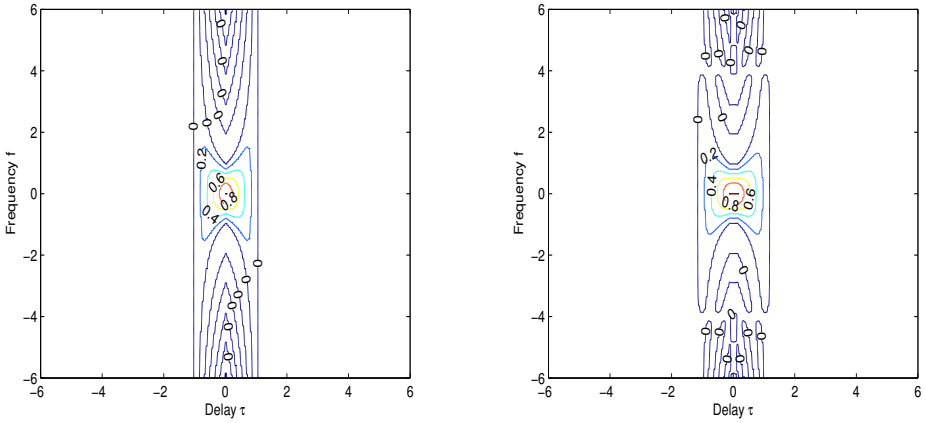

(a) No cyclic prefix (b) Cyclic prefix $\frac{T_g}{T_0} = \frac{1}{5}$

Figure 10: Ambiguity function of rectangular prototype (contour, step=0.2).

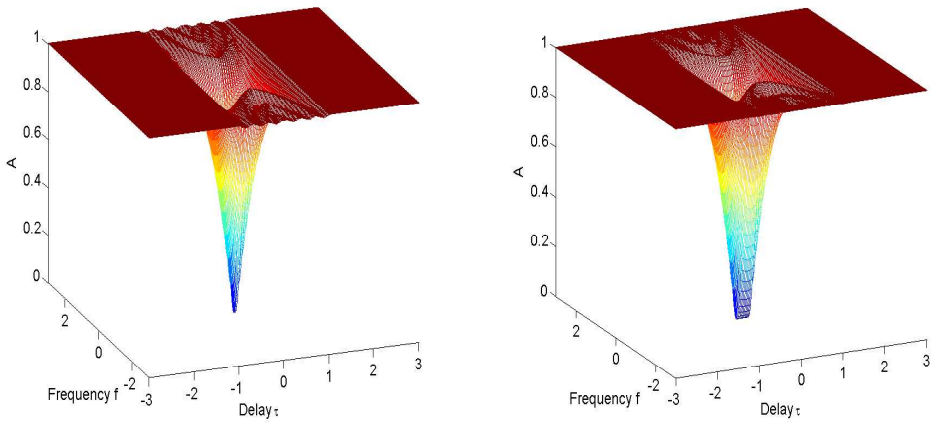

(a) No cyclic prefix (b) Cyclic prefix $\frac{T_g}{T_0} = \frac{1}{5}$

Figure 11: Interference function of rectangular prototype.

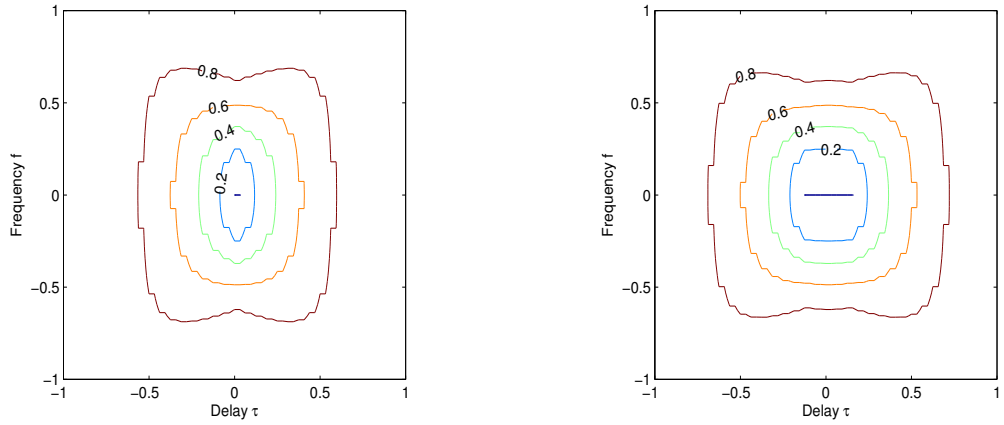

(a) No cyclic prefix

(b) Cyclic prefix $\frac{T_g}{T_0} = \frac{1}{5}$

Figure 12: Interference function of rectangular prototype (contour, step=0.2).

- Observation window length: 12 time and frequency shifts, i.e., $t \in [-6\tau_0, 6\tau_0]$ and $f \in [-6\nu_0, 6\nu_0]$
- Samples per time and frequency shift: 32
- Figures: axes normalized by τ_0 and ν_0 respectively

All the prototype functions mentioned in Sec. 3.2 are derived using these parameters.

5.2.1 Half Cosine Function

As half cosine prototype function and its dual form has the same orthogonality and TFL property but has the time and frequency axes shifted, only the half cosine function in the time domain, i.e. described in eq. (22), are treated here. It has a smaller power leakage along the time axis than the frequency axis, as shown in Fig. 13. Its dual form will of course have the opposite property as only the axes are interchanged.

5.2.2 IOTA function

The nearly *isotropic* property of the IOTA function is shown in Fig. 14. Compared with rectangular and half cosine pulses, IOTA function has a larger and smoother top on the mountain of ambiguity function (or equivalently bottom in the valley of the interference function), and therefore has stronger time and frequency dispersion immunity. $*$ indicate the position of the neighboring lattice points that belong to the same sub-lattice(cf. eq. (19) and Fig. 3), where the ambiguity function has extremely low value (-170 dB), as shown in Fig. 15. One thing to notice is that these lattice points with a distance of $2\tau_0$ or $2\nu_0$ from the origin ($(0, \pm 2)$ and $(\pm 2, 0)$) will have larger power leakage than these points whose distance is $2\sqrt{\tau_0^2 + \nu_0^2}$ $(\pm 2, \pm 2)$. It is coincident with our intuition.

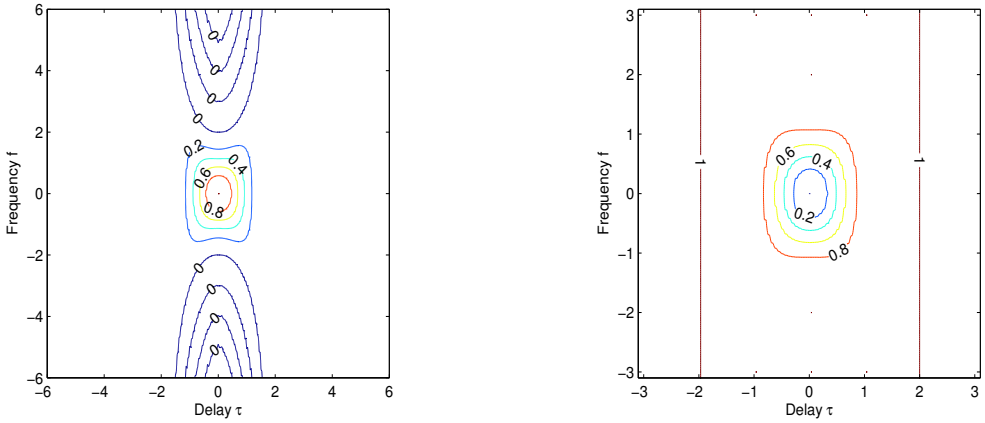

(a) Auto-ambiguity function (b) Interference function

Figure 13: Half cosine prototype (contour, step=0.2).

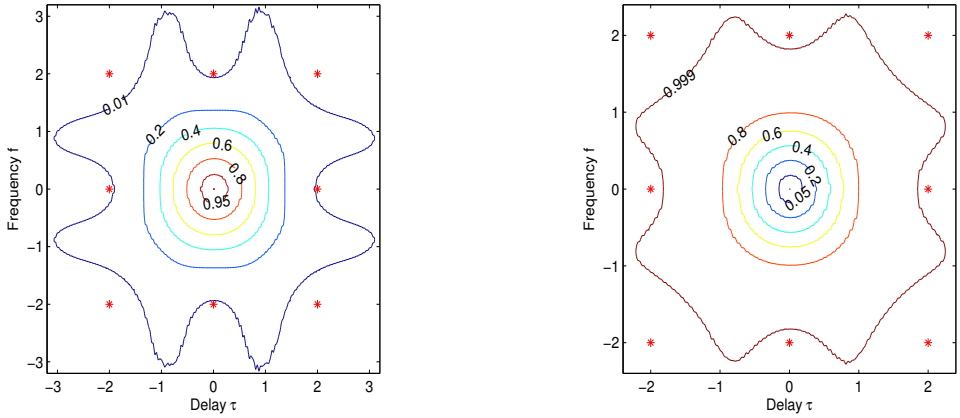

(a) Auto-ambiguity function (b) Interference function

Figure 14: IOTA prototype.

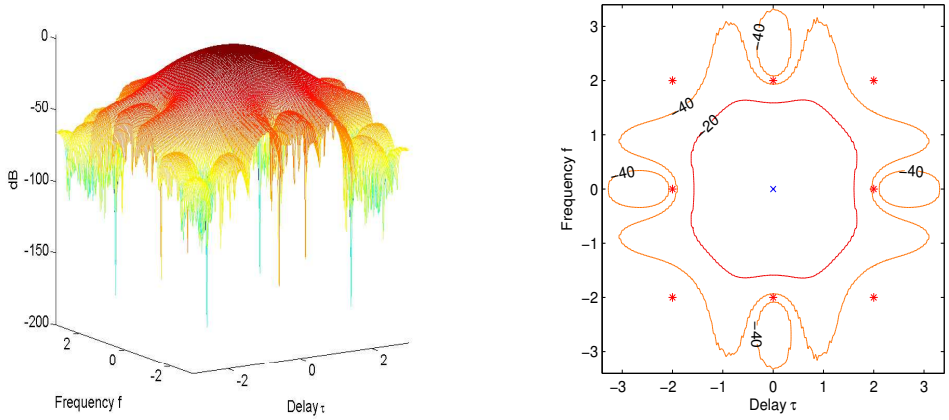

(a) Amplitude [dB] (b) Contour plot [dB]

Figure 15: Ambiguity function of IOTA prototype [dB], $*$ is -170 dB and $\times$ is 0 dB.

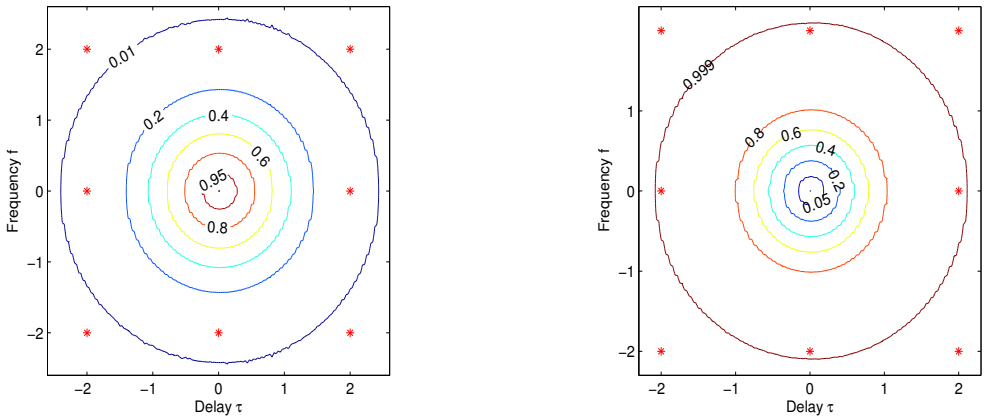

(a) Auto-ambiguity function (b) Interference function

Figure 16: Gaussian prototype with $\alpha = 1$.

5.2.3 Gaussian Function

The Gaussian function is very well localized in time and frequency plane, as shown in Fig. 16. It has a better localization than IOTA function but larger power leakage to neighboring points due to the lack of orthogonality.

5.2.4 Extended Gaussian Function

Two examples of the EGF function are concerned here, $\alpha = 0.265$ and $\alpha = 3.774$, which are the dual functions of each other, as shown in Fig. 17 and Fig. 18. With the IOTA function in between, we get an impression how the EGF function will behave as α increases from 0.265 to 3.774. When we have small α, the pulse tends to be more horizontally (along time axis) stretched and with large α, it tends to be more vertically (along frequency axis) stretched. As a result can we adjust the value of α to adopt most suitable pulse shapes,

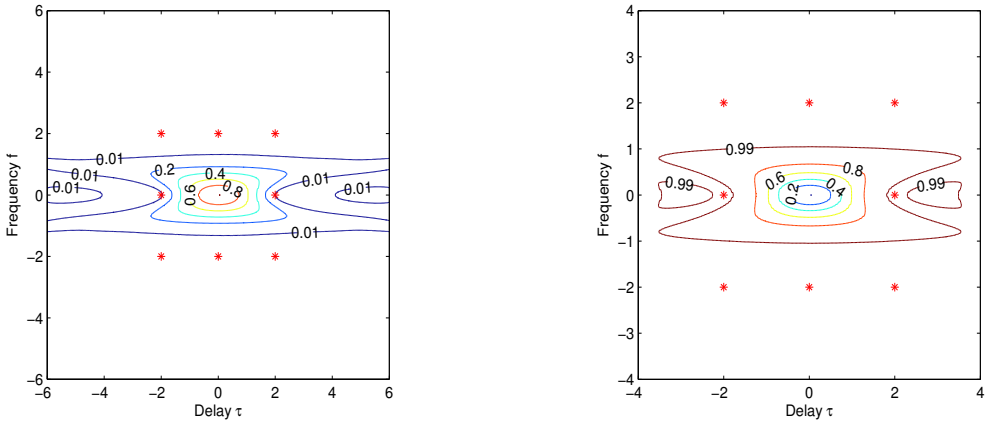

(a) Auto-ambiguity function (b) Interference function

Figure 17: EGF prototype with $\alpha = 0.265$.

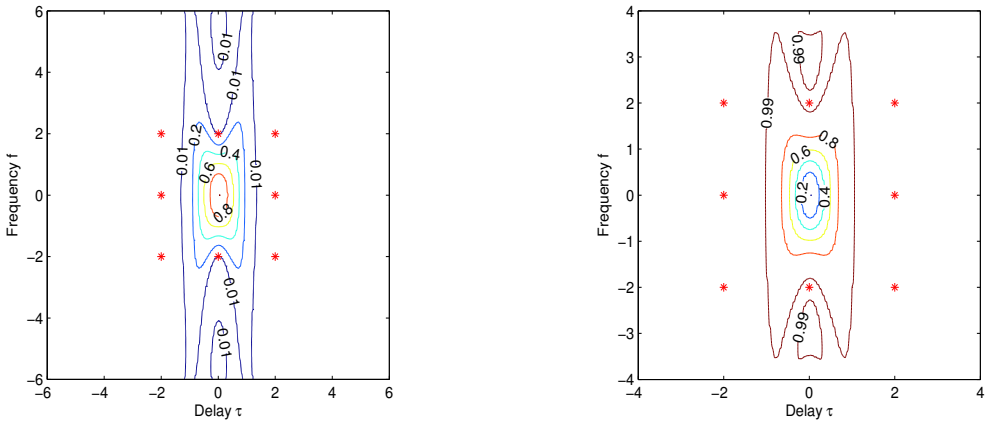

(a) Auto-ambiguity function (b) Interference function

Figure 18: EGF prototype with $\alpha = 3.774$.

as shown in Fig. 4, to the current channel realization.

5.3 Time Frequency Localization

Regarding equation (40), a three dimensional plot as well as a two dimensional contour plot is presented by utilizing the IOTA prototype function. Here the data transmitted on each basis function is ignored for simplicity. These pulses on lattice points with distance $2\tau_0$ or $2\nu_0$ have negative envelope due to the phase factor $e^{j\frac{\pi}{2}(m+n)}$ which equals to -1 when either $|m|$ or $|n|$ equals to 2, but not both. 0 is achieved at the boundary of each lattice grid and therefore no interference will be introduced by neighbors as long as the normalized time or frequency dispersion is less than 2.

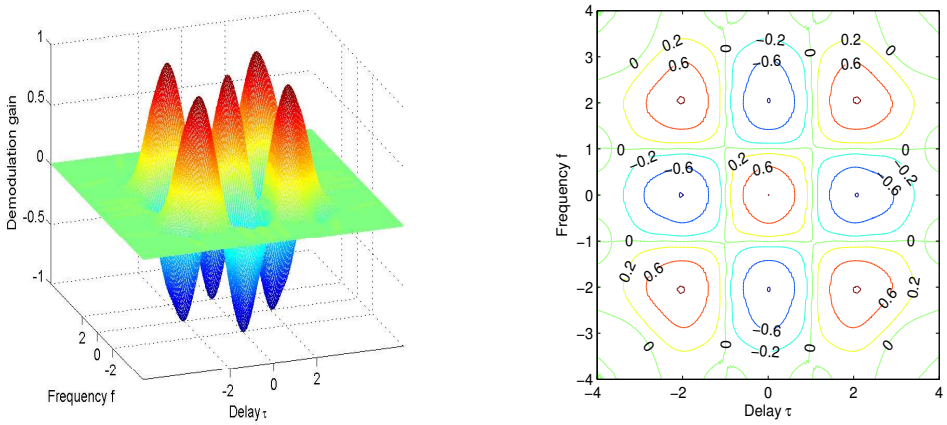

(a) Demodulation gain (b) Contour plot

Figure 19: Demodulation gain of OFDM/OQAM system.

5.4 Heisenberg Parameter ξ

To compare the localization property of different pulses and have a quantitive idea about it, the Heisenberg parameter ξ for each pulse is calculated with two different set of parameters.

Parameters	Rectangular*	Half cosine	IOTA	Gauss	EGF** ($\alpha = 3.774$)
$t, f \in [-6, 6]$	0.3457	0.8949	0.9769	1.000	0.7010
$t, f \in [-40, 40]$	0.1016	0.8911	0.9769	1.000	0.6876

* For rectangular pulse, $\Delta f^2 = \int \sin^2(wf)df = \infty$ and therefore $\xi = 0$ in theory.
** For EGF pulse, $\xi(\alpha) = \xi(1/\alpha)$ and it will steadily increase to its maximum as α approaches 1 from either direction.
The Gauss pulse achieves the maximum of ξ and therefore has the best TFL property. The IOTA pulse shows satisfied localization which is the maximum of ξ among these EGF functions [11].

6 Conclusions

6.1 Conclusion

In this report, we provide a comparative study of state-of-the-art pulse shaping OFDM techniques with orthonormal analysis and synthesis basis. Two main categories, OFDM/QAM and OFDM/OQAM are intensively reviewed. Various prototype functions, such as rectangular, half cosine, IOTA functions and EGF with diverse time frequency localization (TFL) are discussed and TFL properties illustrated by ambiguity function and interference function are provided by simulation results.

By adaptively exploiting different prototype functions with diverse TFL property, dynamic spectrum allocation can be achieved in a more natural way, since the transmitter and receiver adapts dynamically to different channel conditions and interference environments so that higher reliability and spectral efficiency can be expected. Also simplified

synchronization can be expected as less sensitivity to time and frequency offset. The results of this research builds up a solid foundation and can be a good start for further research targeting to revolutionize future wireless communication.

6.2 Further Work

The TFL property can be improved by giving up the orthogonality of the pulses. As an orthogonal basis is not necessary for perfect reconstruction of the original signal, this extra restriction will limit the field for searching for the optimal pulse shapes. By using bi-orthogonal basis instead of an orthogonal one, a so called Non-Orthogonal FDM (NOFDM) [15] or Bi-orthogonal FDM (BFDM) [3, 16] is invented. Although the orthogonal basis functions are optimal in AWGN channels, in time and frequency dispersive channels, the non-orthogonal basis functions, which should necessarily form an (incomplete) Riesz basis [15], turn out to be optimal for the reason that they tend to be more robust against frequency-selective fading and having faster frequency domain decay.

Discarding the orthogonality restriction gives us new degrees of freedom: the synthesis (transmit) pulses can be different from the analysis (receive) pulses, but bi-orthogonality is kept. This allows design of much better pulse shapes. This new freedom, however, will increase the sensitivity to AWGN, since we don't have orthogonal basis functions any more on the transmitter or the receiver sides. Such a trade off between AWGN behavior and ISI/ICI performance always exists in NOFDM/BFDM systems and a general framework which allows fine-tuning the balance between AWGN sensitivity and ISI/ICI robustness is expected to adaptively adjust the pulse shapes according to the channel characteristics.

Another way to enhance the robustness of multicarrier modulation systems against ISI/ICI is to resort to general lattice grids (called Lattice OFDM (LOFDM) in accordance with [17]). With a well designed lattice, say the hexagonal lattice, one can pack the symbols more dense with a given interference that is determined by the distance between adjacent time-frequency points, which is initially fixed by the symbol period and the carrier frequency separation when rectangular grids are used.

Applications of the optimal pulse shaping FDM in the context of MIMO systems, which is of much importance and special interest, is still a very new research area with almost no published contributions.

Appendix

A Proof of Orthogonalization Operator $\mathcal{O}_a$

Apply the Fourier transform operator $\mathcal{F}$ to (17) and set the time parameter $\tau = 0$, we get

$$A_y(0,\nu) = \mathcal{F}\left\{\gamma_y(0,t)\right\} = \mathcal{F}\left\{|y(t)|^2\right\}. \tag{44}$$

Construct an infinite summation regarding $y(t) = \mathcal{O}_a x(t)$ that is given by (27), we get

$$\begin{aligned} a\sum_{m=-\infty}^{\infty}\gamma_y(0,t-ma) &= a\sum_{m=-\infty}^{\infty}|y(t-ma)|^2 \\ &= \sum_{m=-\infty}^{\infty}\frac{|x(t-ma)|^2}{\sqrt{\sum_{k=-\infty}^{\infty}|x(t-ka-ma)|^2\sum_{l=-\infty}^{\infty}|x(t-la-ma)|^2}} \end{aligned} \tag{45}$$

where

$$\sum_{k=-\infty}^{\infty}|x(t-ka-ma)|^2 = \sum_{l=-\infty}^{\infty}|x(t-la-ma)|^2 = \sum_{p=-\infty}^{\infty}|x(t-pa)|^2 \tag{46}$$

whose value is only depending on the function x, time instance t and the positive factor a, and therefore has nothing to do with the summation index (no matter whether m, or k, l, etc. is used). This simplifies (45) and the summation now becomes

$$a\sum_{m=-\infty}^{\infty}\gamma_y(0,t-ma) = \sum_{m=-\infty}^{\infty}\frac{|x(t-ma)|^2}{\sum_{p=-\infty}^{\infty}|x(t-pa)|^2} = \frac{\sum_{m=-\infty}^{\infty}|x(t-ma)|^2}{\sum_{p=-\infty}^{\infty}|x(t-pa)|^2} = 1 \tag{47}$$

By introducing the Dirac's delta function $\delta(t)$ and the convolution operator $*$, (47) can be rewritten as

$$a\sum_{m=-\infty}^{\infty}\gamma_y(0,t-ma) = a\sum_{m=-\infty}^{\infty}\delta(t-ma)*\gamma_y(0,t) = 1 \tag{48}$$

Apply the Fourier transform on both sides and notice that [10]

$$\begin{aligned} \mathcal{F}\left\{\sum_{m=-\infty}^{\infty}\delta(t-ma)\right\} &= \frac{1}{a}\sum_{m=-\infty}^{\infty}\delta(\nu-\frac{m}{a}),\ a>0 \\ \mathcal{F}\left\{1\right\} &= \delta(\nu) \\ \mathcal{F}\left\{x(t)*y(t)\right\} &= X(\nu)Y(\nu) \end{aligned} \tag{49}$$

we can get

$$\sum_{m=-\infty}^{\infty}\delta(\nu-\frac{m}{a})A_y(0,\nu) = \delta(\nu) \tag{50}$$

which gives out straightforward $A_y(0,0) = 1$ and $A_y(0,\frac{m}{a}) = 0\ \forall m \neq 0$. Proved.

B EGF Coefficients Calculation

According to [11], the coefficients d_{k,α,ν_0} can be expressed as

$$\begin{aligned} d_{k,\alpha,\nu_0} &= \sum_{l=0}^{\infty} a_{k,l} e^{-\frac{\alpha\pi l}{2\nu_0^2}},\ 0 \le k \le \infty \\ &\approx \sum_{j=0}^{j_l} b_{k,j} e^{-\frac{\alpha\pi}{2\nu_0^2}(2j+k)},\ 0 \le k \le K \end{aligned} \tag{51}$$

where $j_l = \lfloor (K-k)/2 \rfloor$ and K is a positive integer which insure an accuracy of $e^{-\frac{\pi\alpha K}{2\nu_0^2}}$ for the approximation due to truncation of the infinity summation.

A list of coefficients $b_{k,j}$ corresponding to $K = 14$, which leads to an accuracy of 10^{-19} for $\alpha = 1$, is present in the following table.

$b_{j,k}$	j (0 to 7)							
	1	$\frac{3}{4}$	$\frac{105}{64}$	$\frac{675}{256}$	$\frac{76233}{16384}$	$\frac{457107}{65536}$	$\frac{12097169}{1048576}$	$\frac{13774755}{4194304}$
	-1	$-\frac{15}{8}$	$-\frac{219}{64}$	$-\frac{6055}{1024}$	$-\frac{161925}{16384}$	$-\frac{2067909}{131072}$	$-\frac{26060847}{1048576}$	
	$\frac{3}{4}$	$\frac{19}{16}$	$\frac{1545}{512}$	$\frac{9765}{2048}$	$\frac{596277}{65536}$	$\frac{3679941}{262144}$	$-\frac{105421227}{16777216}$	
	$-\frac{5}{8}$	$-\frac{123}{128}$	$-\frac{2289}{1024}$	$-\frac{34871}{8192}$	$-\frac{969375}{131072}$	$-\frac{51182445}{4194304}$		
k	$\frac{35}{64}$	$\frac{213}{256}$	$\frac{7797}{4096}$	$\frac{56163}{16384}$	$\frac{13861065}{2097152}$	$-\frac{139896345}{8388608}$		
0	$-\frac{63}{128}$	$-\frac{763}{1024}$	$-\frac{13875}{8192}$	$-\frac{790815}{262144}$	$-\frac{23600537}{4194304}$			
to	$\frac{231}{512}$	$\frac{1395}{2048}$	$\frac{202281}{131072}$	$\frac{1434705}{524288}$	$-\frac{142044345}{16777216}$			
14	$-\frac{429}{1024}$	$-\frac{20691}{32768}$	$-\frac{374325}{262144}$	$-\frac{5297445}{2097152}$				
	$\frac{6435}{16384}$	$\frac{38753}{65536}$	$\frac{1400487}{1048576}$	$-\frac{1458219}{4194304}$				
	$-\frac{12155}{32768}$	$-\frac{146289}{262144}$	$-\frac{2641197}{2097152}$					
	$\frac{46189}{131072}$	$\frac{277797}{524288}$	$\frac{20050485}{16777216}$					
	$-\frac{88179}{262144}$	$-\frac{2120495}{4194304}$						
	$\frac{676039}{2097152}$	$\frac{4063017}{8388608}$						
	$-\frac{1300075}{4194304}$							
	$\frac{5014575}{16777216}$							

As for coefficients $d_{k,1/\alpha,\tau_0}$, the dual form of d_{k,α,ν_0}, it is easy to calculate them just by replacing the corresponding items and following the above procedure.

Acknowledgment

This work is partly supported by the center of Wireless@KTH under small project "Next Generation FDM".

References

[1] B. le Floch, M. Alard and C. Berrou, "Coded Orthogonal Frequency Division Multiplex," *Proceedings of the IEEE*, vol. 83, pp. 982–996, June 1995.

[2] H. Bölcskei, P. Duhamel, and R. Hleiss, "Design of pulse shaping OFDM/OQAM systems for high data-rate transmission over wireless channels," in Proc. of *IEEE International Conference on Communications (ICC)*, Vancouver, BC, Canada, June 1999, vol. 1, pp. 559–564.

[3] D. Schafhuber, G. Matz, and F. Hlawatsch, "Pulse-shaping OFDM/BFDM systems for time-varying channels: ISI/ICI analysis, optimal pulse design, and efficient implementation," in Proc. of *IEEE International Symposium on Personal, Indoor and Mobile Radion Communications*, Lisbon, Portugal, Sep. 2002, pp. 1012–1016.

[4] A. Vahlin and N. Holte, "Optimal finite duration pulse for OFDM," *IEEE Transactions on Communications*, vol. 44, pp. 10–14, Jan. 1996.

[5] R. Haas and J.-C. Belfiore, "A time-frequency well-localized pulse for multiple carrier transmission," *Wireless Personal Communications*, vol. 5, pp. 1–18, Jan. 1997.

[6] TIA Committee TR-8.5, "Wideband Air Interface Isotropic Orthogonal Transform Algorithm (IOTA) –Public Safety Wideband Data Standards Project – Digital Radio Technical Standards," TIA-902.BBAB (Physical Layer Specification, Mar. 2003) and TIA-902.BBAD (Radio Channel Coding (CHC) Specification, Aug. 2003) http://www.tiaonline.org/standards/

[7] M. Bellec and P. Pirat, "OQAM performances and complexity," *IEEE P802.22 Wireless Regional Area Network (WRAN)*, Jan. 2006. http://www.ieee802.org/22/Meeting_documents/2006_Jan/22-06-0018-01-0000_OQAM_performances_and_complexity.ppt

[8] S. Signell, "IOTA Functions and OFDM," Slides and MATLAB code, 2003-2004.

[9] S. Mallat, *A Wavelet Tour of Signal Processing, Second Edition*, Academic Press, 1999.

[10] L. Råde and B. Westergren, *Mathematics Handbook for Science and Engineering*, Studentlitteratur, 2004.

[11] M. Alard, C. Roche, and P. Siohan, "A new family of function with a nearly optimal time-frequency localization," *Technical Report of the RNRT Project Modyr*, 1999.

[12] P. Siohan and C. Roche, "Cosine-Modulated Filterbanks Based on Extended Gaussian Function," *IEEE Transactions on Signal Processing*, vol. 48, no. 11, pp. 3052–3061, Nov. 2000.

[13] N.J. Baas and D.P. Taylor, "Pulse shaping for wireless communication over time- or frequency-selective channels", *IEEE Transactions on Communications*, vol 52, pp. 1477–1479, Sep. 2004.

[14] P. Siohan, C. Siclet and N. Lacaille, "Analysis and design of OFDM/OQAM. systems based on filterbank theory" *IEEE Transactions on Signal Processing*, vol. 50, no. 5, pp. 1170-1183, May 2002.

[15] W. Kozek, A.F. Molisch, "Nonorthogonal pulseshapes for multicarrier communications in doubly dispersive channels," *IEEE Journal on Selected Areas in Communications*, vol. 16, no. 8, pp. 1579–1589, Oct. 1998.

[16] P. Schniter, "On the design of non-(bi)orthogonal pulse-shaped FDM for doubly-dispersive channels," in Proc. of *IEEE International Conference on Acoustics, Speech, and Signal Processing (ICASSP)*, Montreal, Quebec, Canada, May 2004, vol. 3, pp. 817–820.

[17] T. Strohmer and S. Beaver, "Optimal OFDM Design for Time-Frequency Dispesive Channels," *IEEE Transactions on Communications*, vol. 51, pp. 1111–1123, Jul. 2003.